Journal of Marine Science and Engineering

MDPI

Article

Past Analogues of Deoxygenation Events in the Mediterranean Sea: A Tool to Constrain Future Impacts

Alan Maria Mancini [1,*], Giacomo Bocci [2], Caterina Morigi [2], Rocco Gennari [1], Francesca Lozar [1] and Alessandra Negri [3]

[1] Earth Sciences Department, Università degli Studi di Torino, 10125 Torino, Italy
[2] Department of Earth Sciences, Università di Pisa, 56126 Pisa, Italy
[3] Department of Life and Environmental Science, Università Politecnica delle Marche, 60122 Ancona, Italy
* Correspondence: alanmaria.mancini@unito.it

Abstract: Human-induced carbon emissions are altering the modern climate, with severe repercussions on ecosystems. Among others, anthropogenic pressure is causing deoxygenation of the bottom water, with the widespread establishment of hypoxic zones in several Mediterranean areas. The geological archives allow investigating past deoxygenation dynamics (sapropel events) and their impact on marine ecosystems. Here, we compare the causes and the evolution of deoxygenation dynamics which occurred during two different time periods (Messinian and Holocene) in different paleoceanographic settings based on their micropaleontological content. The Messinian sapropel events are the result of increased export productivity during a relatively cold and arid context, triggering bottom anoxic conditions. The Holocene sapropel formed in response to weakening/stopping of the thermohaline circulation due to increasing temperature and freshwater input. Our results suggest that the deoxygenation dynamics in the Mediterranean in the near future will not follow the trend characteristic of the Holocene deep-sea sapropel because of the predicted drying trend. Differently, the paleoceanographic setting triggering the Messinian shallow-sea sapropels is comparable with the modern situation in different Mediterranean areas, where human-induced eutrophication is promoting deoxygenation. Based on these results, we suggest that the patchy deoxygenation trend in the Mediterranean Sea caused by climate warming may lead to a drastic change in the ecosystem services which would likely impact human activities.

Keywords: sapropel; anoxia; calcareous nannofossils; foraminifers; climate change; marine productivity; thermohaline circulation

Citation: Mancini, A.M.; Bocci, G.; Morigi, C.; Gennari, R.; Lozar, F.; Negri, A. Past Analogues of Deoxygenation Events in the Mediterranean Sea: A Tool to Constrain Future Impacts. *J. Mar. Sci. Eng.* **2023**, *11*, 562. https://doi.org/10.3390/jmse11030562

Academic Editor: Weidong Zhai

Received: 7 February 2023
Revised: 2 March 2023
Accepted: 3 March 2023
Published: 6 March 2023

1. Introduction

During post-industrial times, human activities have severely impacted the biogeochemical cycles and ecosystems through exceptional emissions of CO_2 into the atmosphere, which has ultimately affected modern climate evolution [1]. Among other environmental factors (i.e., ocean fertilisation), the current warming trend is expected to lead the global ocean to an overall oxygen deficiency [2]; similarly, the semi-enclosed Mediterranean Sea is expected to face this issue [3]. This is due to the effect of warmer temperatures, which cause a decrease in the oxygen solubility of seawater, a weakening of the thermohaline circulation strength [2], and an increase in the oxygen consumption by prokaryotic metabolism [4,5]. During the last 50 years, the global oxygen inventory in the open ocean has been reduced by ~2% [6] and the coastal water of more than 500 sites reported oxygen concentration < 2 mg liter^{-1} [7], which is the threshold often used to define hypoxia. Globally, the oxygen minimum zone (OMZ) in the period 1990–2008 has expanded by an area comparable to the size of the European Union (4.5 million km^2) [8]. The expansion of the OMZ is a recurrent feature associated with warming in the geological record, such as those which occurred during the Paleocene–Eocene thermal maximum (~55.5 Ma), with

severe consequence for marine biota [9,10]. The condition of increasing oxygen starvation is negatively impacting benthic biocenosis [11], and zooplankton and fish production [12]. Furthermore, the combined effect of warming and deoxygenation have a synergic negative effect on marine biocenosis, called "oxythermic stress" [13]. A negative synergic effect was also hypothesized for the combined impact of ocean acidification and deoxygenation in some molluscs and fish taxa [14]. Therefore, understanding the main variables involved in the current climate change is crucial to better constrain, and possibly predict, future impact scenarios. In this regard, the study of the past is a precious resource to understand long-term environmental dynamics for deoxygenation trends and depict future impact scenarios. The Mediterranean Sea is a key area to investigate this issue because in the geological past it experienced widespread deoxygenation events recorded by distinct dark layers called sapropels. According to [15], sapropels are discrete layers > 1 cm thick deposited in open marine pelagic realms and containing more than 2% organic carbon. The sapropel events can be seen as perturbations of the carbon and oxygen cycles; indeed, these events record an increase in organic carbon burial in response to anoxic conditions. Sapropels are cyclically deposited in the Mediterranean Sea in response to specific climate, oceanic circulation, and biogeochemical cycling [16,17] controlled by variation in the Earth's orbital parameters [18]. Although [19] proposed a single mechanism explaining the sapropel occurrence in the Mediterranean throughout the Neogene and Quaternary, the authors of [20] propose different paleoceanographic settings for the Messinian sapropel deposition in the shelf setting of the Sorbas Basin, located in the western Mediterranean (Figure 1). Differently from the coeval deep-sea sapropel deposited in the eastern Mediterranean, the anoxic condition for sapropel deposition in the western Mediterranean was triggered by natural variation in primary productivity and export regimes favoured by restricted condition and paced by the precession index [20]. The bottom anoxic condition was a response of the ecosystem to eutrophication, similar to that currently occurring in different Mediterranean shelves and enclosed areas caused by human activity [21–25].

The aim of this paper is therefore to compare sapropels deposited in different times and oceanographic settings (Messinian shallow western Mediterranean Sea vs. Holocene deep eastern Mediterranean Sea) to find the best past analogue of the current deoxygenation dynamic in the Mediterranean Sea, allowing to obtain clues for possible future impacts.

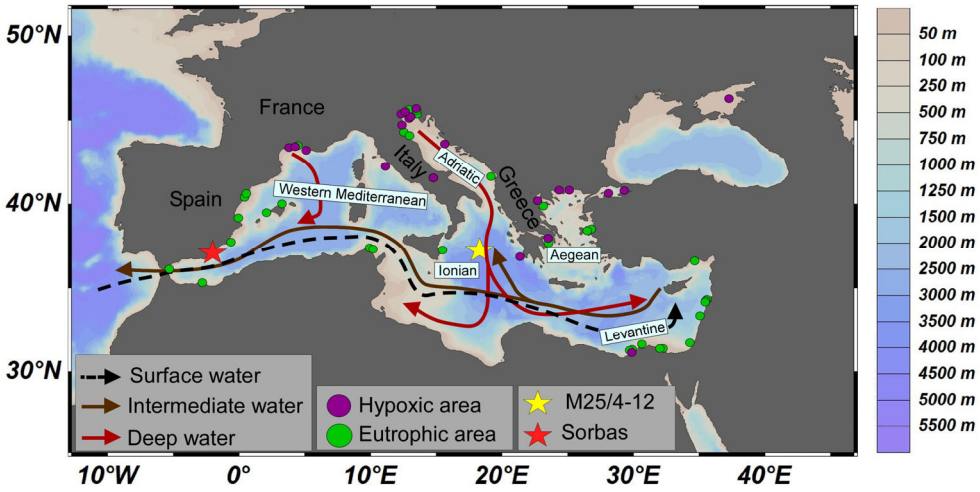

Figure 1. Map of the studied area. Yellow star indicates the M25/4-12 core location; red star indicates the Sorbas Basin location. Arrows indicate the major currents and their depth in the water column. Purple and green circles identify the location of hypoxic and eutrophic areas recorded from 1960 to 2010 in the coastal zones of the Mediterranean Sea (modified from UNEP-MAP [22] and [24]). Map

obtained using the Ocean Data View software [26], (https://odv.awi.de, accessed on 02 December 2022).

2. Oceanographic and Climatic Framework

The Mediterranean is a semi-enclosed sea characterised by a specific hydrographic regime. The Strait of Sicily virtually separates the Mediterranean Sea into two sub-basins, the eastern and western Mediterranean with different processes and characteristics of the water masses [17]. The eastern sub-basin is characterised by three distinct water masses: the Atlantic Modified Water (AMW; 0 to ~200 m), the Levantine Intermediate Water (LIW, 200–500 m), and the eastern Mediterranean Deep Water (EMDW; <500 m). The AMW flows eastward from the Strait of Sicily progressively gaining salinity as a result of the warm and dry weather in this part of the basin; near the Turkish coast, during winter, the cooling causes buoyancy loss to the AMW which sinks, forming the LIW which moves west towards the Adriatic Sea and the western Mediterranean through the Strait of Sicily. The LIW is underlying the EMDW, which moves west through the Strait of Sicily and a part is mixed with the cold water originating in the Adriatic shelf, forming the Adriatic Deep Water (ADW). The Western Mediterranean Deep Water (WMDP) forms during winter in the Gulf of Lyon and is coupled with an effective Bernoulli aspiration through the Gibraltar Strait [17]. Due to these thermohaline processes, the eastern Mediterranean is more sensitive to oxygen deficiency at the sea bottom compared to the western Mediterranean.

Future projections [27–29] indicate a scenario characterized by a progressively weaker thermohaline circulation, due to intense stratification driven by warming of the Mediterranean water. In addition, the freshening of the Atlantic Ocean due to Arctic ice melting could potentially increase the basin stratification by decreasing the AMW density. The main impact of this circulation change is on the oxygen content of the water column with possible negative impacts on marine ecosystems. In addition, the weakening of thermohaline circulation is coupled with eutrophication in several coastal and enclosed areas [22,23], increasing the production and export of biomass and consequently the consumption of the dissolved oxygen.

Sapropel and Deep-Sea Anoxia

Major climate oscillations, such as the alternation of ice ages and interglacials, are induced by seasonal and latitudinal changes in the amount of insolation; the latter is caused by variations in the movement of the Earth's rotational axis (precession and obliquity) modulated by eccentricity [30]. At the same time scale, in the Mediterranean Sea, anoxic events caused the periodic deposition of sapropel during the past 15 Ma [17,31]. Sapropels have been recovered in sediment cores throughout the Mediterranean Basin and in onshore marine successions around the basin, showing a pattern related to the precession cyclicity (~21,000 years) [17]. They were discovered during the Swedish Deep Sea Expedition (1948) and their deposition is related to glacial–interglacial cycles [32]: the combination of warm, low-density superficial water resulted in the stratification of the water column and in the stagnation of bottom waters. Later, it was pointed out that sapropels are linked to reduced oxygen supply triggered by limited deep-water circulation and/or increased oxygen demand due to enhanced primary productivity, or a variable combination of the two [17 and references therein]. Sapropels represent some of the best-documented marine anoxia-driven carbon burial events, well developed in times of maximum eccentricity (high seasonality), and often missing during times of minimum eccentricity (low seasonality) [17 and references therein].

Literature on the Quaternary sapropels shows that the weakening/shutdown of the LIW exerted first-order control on their formation [17,33]. Today, the LIW supplies enough salt to the Adriatic and Aegean Sea for the formation of the EMDW in winter [34]. This water mass is critical for the Mediterranean thermohaline circulation, supplying oxygen to the deep basin during events of dense water formation. At the times of the most

recent sapropels' formation, the African monsoon shifted in response to orbital cycles and increased the Nile discharge, which drastically decreased the LIW formation (i.e., freshening of the Levantine basin), and in turn, decreased the EMDW formation [17 and references therein]. Therefore, the deterioration of the thermohaline circulation is thought to play a primary role in the sapropel deposition during the Plio-Quaternary, through variation in the freshwater influx and nutrient supply to the basin.

As for the Messinian sapropels, they represent the sedimentary response to restricted condition and, as in the case of the Plio-Quaternary sapropels, their sedimentation followed precession-induced climatic fluctuations [35], allowing the tuning of the sapropel (stratigraphic) midpoint with precession minima—insolation maxima [36,37]. Indeed, the progressive basin restriction of the Mediterranean Basin was the result of tectonic processes that reduced the water exchange between the Mediterranean and the Atlantic through the paleo Gibraltar Strait [38]. The restriction of the Mediterranean Basin proceeded by steps, which were dated at 7.19, 6.7, 6.4, 6.1, and 5.99 Ma [20,39,40]. Each of these steps marked a deterioration of the bottom water circulation, which increased the bottom water residence time leading to oxygen deficiency at the seafloor [39–41]. The eastern Mediterranean was already subjected to sapropel deposition since the Langhian, but their formation was typical of the eccentricity maxima [31,42]. Starting from 7.19 Ma, the restriction allowed their formation also during eccentricity minima, when oscillations of the insolation were less extreme [19,41,43]. Indeed, during the late Miocene, the eastern Mediterranean was more affected by runoff (from the north African rivers) compared to the western part (Figure 2) and to the modern situation [44]. In addition, freshwater spill from the Paratethys [45] further enhanced the water column stratification in the eastern part of the basin (Figure 2). The second restriction step (6.7 Ma) marked the onset of cyclical sapropel deposition also in the western Mediterranean (Figure 2) [46]. In a small peripheral basin of the western Mediterranean (Sorbas Basin, 37°05′49″ N–2°03′19″ W; Figures 1, 2 and 3A–C), the cyclical sapropel deposition occurred on the shelf and was triggered by enhanced organic carbon export to the seafloor in response to high productivity in the water column [20], suggesting a different mechanism for the sapropel formation in the different Mediterranean sub-basins.

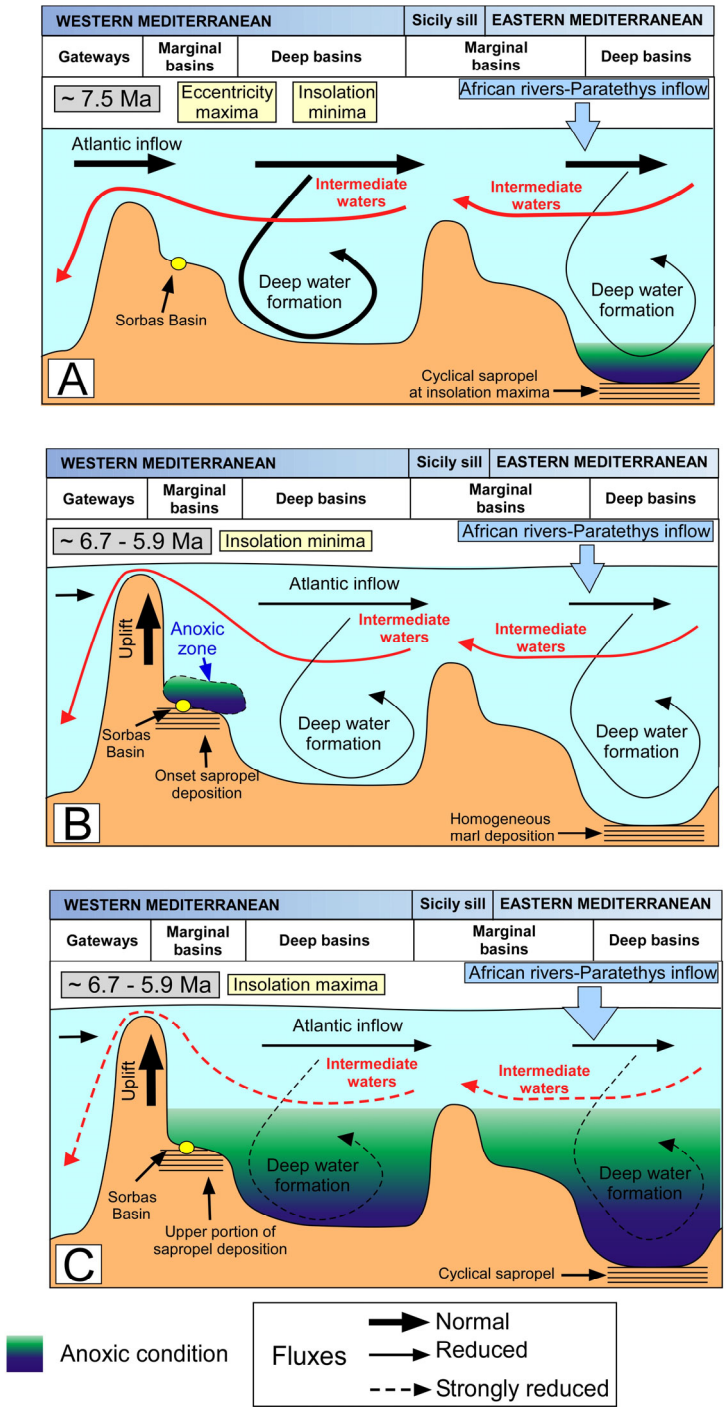

Figure 2. Sketch showing the Late Miocene thermohaline circulation in the Mediterranean in relation with the deposition of sapropel. (**A**): Thermohaline circulation and sapropel deposition (constrained from present circulation pattern and on the basis of the Messinian sedimentary succession) [34,39,41,43,44,47,48], when open marine condition and vigorous thermohaline circulation prevailed. B and C: Thermohaline circulation after the restriction step dated at ~6.7 Ma [41,43,44,47–51] during insolation minima (**B**) and insolation maxima (**C**) periods. Sketch modified after [41].

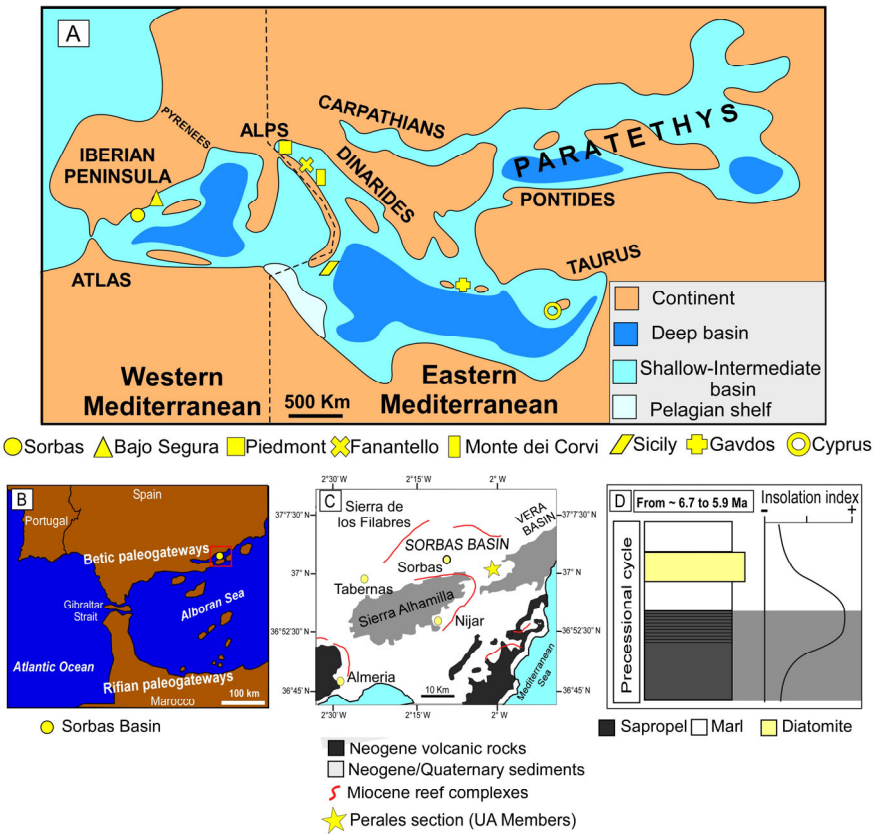

Figure 3. (**A**): Messinian paleogeography of the Mediterranean with the principal localities in which sapropels were recorded. Modified after [52]. Data from [19, 40, 47–49,51,53–55]. (**B**): Sorbas Basin paleogeographic location from ~6.7 to 5.9 Ma, modified after [56,57]. (**C**): Geological map of southeast Spain showing the location of the studied interval. (**D**): Basic sedimentary cycle of the Sorbas Basin recording precessional footprint and its relationship with insolation index [58].

3. Material and Methods

3.1. The Sapropels of the Sorbas Basin

The Sorbas Basin forms part of the Betic Corridor, which was one of the northern Atlantic–Mediterranean connections during the late Miocene (Figure 3B). The basin is elongated and bounded by the Sierra de Filabres and by the Sierra Alhamilla to the north and to the south, respectively (Figure 3C). The Messinian is represented by the Abad Member, which was deposited in the basin depocenter and consists of hemipelagic sediment [59]. Based on the different lithologies, the Abad Member can be divided into two units: the Lower Abad (LA), with the base at approximately the Tortonian/Messinian boundary (~7.2 Ma) and the Upper Abad (UA), starting at 6.7 Ma [59]. Both units record the precessional signal through different pattern of the lithological expression and of the micropaleontological content. The LA is characterized by an alternation of massive whitish marls and massive grey marls [59]; the UA deposits are characterized by a quadripartite cycle (sapropel—marl—diatomite—marl). A total of 34 cycles are present in the UA [49].

The sedimentary cyclicity of the Sorbas Basin from 6.7 to 5.9 Ma (UA Member) was studied in detail by means of micropaleontological (foraminifera and calcareous nannofossil) and isotopic analyses [20,49,60–62] to reconstruct the main paleoenvironmental change related with precessional fluctuations. The age model relied on magnetostratigraphy, biostratigraphy, and cyclostratigraphy [49,59]. We used the depositional model proposed in [20], which compiled all the available datasets presented in the literature regarding the UA [20,49,60,61]. The depositional model was based on high resolution (less than

0.4 Ka resolution) studies conducted on four precession-driven lithological cycles (6.62–6.54 Ma) [60,61]; and with lower resolution studies (3.3–2.0 Ka resolution) [20,49]. The temperature index was calculated [46,49,60] considering the fluctuation of the planktic foraminifera which proliferate in warm-oligotrophic water (*Globigerinoides obliquus*, *G. sacculifer*, *Orbulina universa*, and *Globoturborotalita apertura*) over the taxa proliferating in cold-eutrophic water (*Globigerina bulloides* and *Turborotalita quinquerloba* and *T. multiloba*) [63,64]. As the benthic foraminiferal association is entirely composed of taxa characteristic of low oxygen and high organic carbon flux to the seafloor, such as the genera *Uvigerina*, *Bolivina*, and *Bulimina* [49,65–67], the variation in the absolute abundance of benthic foraminifera (number of specimens/gram of dried sediment) reflects organic carbon and oxygen availability at the seafloor [20,68,69]. Therefore, the benthic foraminiferal absolute abundance is used as an index of bottom oxygenation to the seafloor. Finally, a DCM index was provided considering the fluctuation in relative abundance of the calcareous nannofossil taxa *Sphenolithus abies,* since this taxon is reported to have similar ecological requirements to the living *Florisphaera profunda*, which proliferates in the lower part of the photic zone [20,70].

3.2. The Sapropel S1 in the M25/4-12 Core

The studied sapropel S1 was described by [71] in the core M25/4-12 (37°58′ N 18°11′ E), collected at 2467 m depth in the Ionian Sea (Figure 1), during the R/V *Meteor* cruise 25/4 (August 1993). In 2013, the sampling was further refined at higher resolution (1 cm pacing). The new data presented here focus on Section 1 of the core (Supplementary Materials S1, Subsection 2.1, Table S1), where 10 AMS ^{14}C datings were provided by the Radiocarbon laboratory at ANU (Australian National University) and calibrated with Marine stage 20 [72].

A total of 35 samples were prepared for micropaleontological investigation, with an overall sample resolution of 1 cm across the S1 and every 5 cm in the remaining part of the section. Standard smear-slides were prepared for the calcareous nannofossil analysis and successively observed at 1250X by polarized light microscopy. For the foraminiferal analysis, we wet-sieved the dried sample, previously weighted, to obtain two size fractions: >150 μm and 150–63 μm. The calcareous nannofossils and foraminiferal relative and absolute (foraminifera only) abundance were calculated following taxonomic identification.

3.3. Micropaleontological-Based Indexes as a Proxy of Deoxygenation Event

We calculated several micropaleontological indexes to compare with previously applied methods for constraining the dynamics of Messinian deoxygenation. These indexes are based on the assumption that the distribution pattern of some taxa is mainly related to selected environmental parameters, such as sea surface temperature and productivity. To this end, a foraminifera-based temperature index was calculated with the formula:

$$W/C_{forams} = \%W/(\%W + \%C)$$

Where C are the cold foraminiferal taxa (*Globorotalia inflata, Globorotalia scitula, Globorotalia truncatulinoides, G. bulloides, Neogloboquadrina dutertrei* and *N. incompta*) and W the warm foraminiferal taxa (*Orbulina universa, Globigerinoides ruber, G. trilobus* and *Globoturborotalita rubescens*), according to [73].

A foraminifera-based productivity index was calculated through the % sum of eutrophic and opportunistic specimens (*G. bulloides*, *Turborotalita quinqueloba* and *Globigerinita glutinata*) according to [73].

A coccolith-based Deep Chlorophyll Maximum (DCM) was calculated based on the abundance fluctuation of *F. profunda*, this taxon being a deep photic zone dweller which shows high abundance when the nutrients are preferentially located in the lower photic zone [71,74]. We calculated the DCM index using the formula (modified after [75]):

$$DCM_{cocco} = \%F/[\%F + \%UPZ]$$

Where F is the *F. profunda* abundance and UPZ are the upper photic zone dweller specimens (in our case, we consider *Emiliania huxleyi*). This index shows how much of the productivity was concentrated in the deep part of the photic zone.

Finally, the benthic foraminiferal absolute abundance is used to track the change in the bottom oxygenation, since their abundance and spatial occurrence is mostly controlled by nutrient and oxygen availability to the seafloor [67].

4. Results

4.1. Micropaleontological Signature of the Sorbas Basin Sapropel

Micropaleontological analyses performed in the Sorbas Basin spanning 6.7–5.9 Ma (UA Member) [46,49,60–62] were recently summarized in [20] (Figure 4), integrating all the available data regarding the sapropel deposited in the UA Member to build a general depositional model explaining the environmental changes associated with the deposition of the different lithologies (Figure 4). The micropaleontological analyses revealed different planktic and benthic assemblages at the sapropel base and in the middle-upper part of the sapropel (Figure 4). At the sapropel base, the prevalence (up to 100% of the assemblage [47]) of cold-eutrophic planktic foraminifera and high benthic foraminiferal abundance (in some cases exceeding 200 specimens g^{-1}) is observed [49,60,61]; conversely, warm-oligotrophic foraminifera and DCM dwellers dominate the middle-upper part of the sapropel Figure 4 [20,49,60,61]. This portion of the sapropel is also laminated and shows scarce or even absent benthic foraminifera. In the upper part of the sapropels, the high abundance (up to 100% of the total assemblage [47]) of warm-lover taxa indicates maximum values of the insolation index.

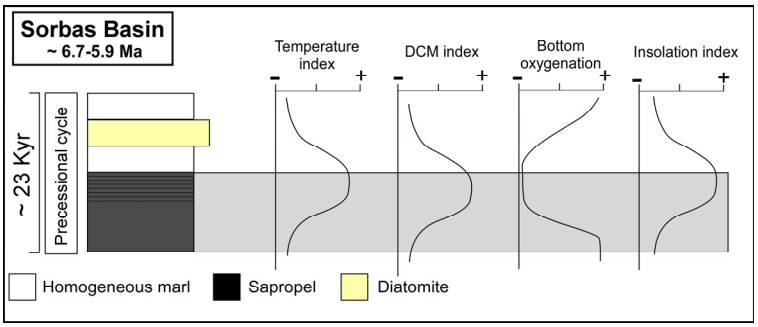

Figure 4. Sketch showing the micropaleontological feature characterising the cyclical sapropel deposition during the Messinian (from 6.7 to 5.9 Ma) in the Sorbas Basin. Data from [46,49,60,61], summarized by [20]. More details in the Section 4.1.

4.2. Micropaleontological Signature of Sapropel S1

Based on the radiometric ages (Figure 5), the studied interval spans from 27.3. BP to the Z1 tephra, corresponding to the Vesuvius eruption (79 A.D.), that is used as an additional data point for the age model. Based on the age model, a greyish interval that we identify as "protosapropel" occurs between 41 cm and 36.5 cm (11.7–10.4 Ka cal. BP) and from 36.5 to 24.5 cm (7.3 Ka cal. BP), the dark colour typical of the sapropel is evident. From 24.5 cm to 20 cm (5.6 Ka cal. BP), the colour turns to light brown/red (Supplementary Materials S1, Subsection 2.1, Figure S1), which corresponds to the oxidized sapropel [76]. Above this interval, between 20 cm and 7 cm the sediment colour is the typical pink characterizing bioturbated hemipelagic sediment, and at the top of the core the Z1 tephra (7–0 cm) [77] occurs. Our stratigraphic log was then correlated with insolation curve at 65° N [58].

Raw micropaleontological results of the studied interval are reported in the Supplementary Materials (S1, subsections 2.2 and 2.3, Figure S2 and S3). Figure 6 summarizes

the main fluctuations observed in the calculated indices: the foraminifera-based temperature index shows low values in the lower portion of the studied interval, where the assemblage was composed of cold-eutrophic taxa (*G. scitula*, *N. incompta* and *G. bulloides*) [73]. This suggests that the Last Glacial Maximum (LGM) falls between 27.6–20.9 Ka cal BP (Figure 5). This index increased below the protosapropel (11.7 Ka cal BP), and in the visible sapropel interval showed higher temperatures than in the overlying and underlying sediment (Figure 5). The foraminifera-based productivity index, although fluctuating, recorded an upward gradually increasing trend, punctuated by a short drop at the top of the visible sapropel. The coccoliths-based DCM proxy recorded a short peak just above the LGM and higher values within the S1 (Figure 5). Finally, the oxygenation index was null in the sapropel and highly fluctuated (from 0 up to 104 specimens g^{-1}, Supplementary Materials S1, paragraph 2.3) below and above it (Figure 5).

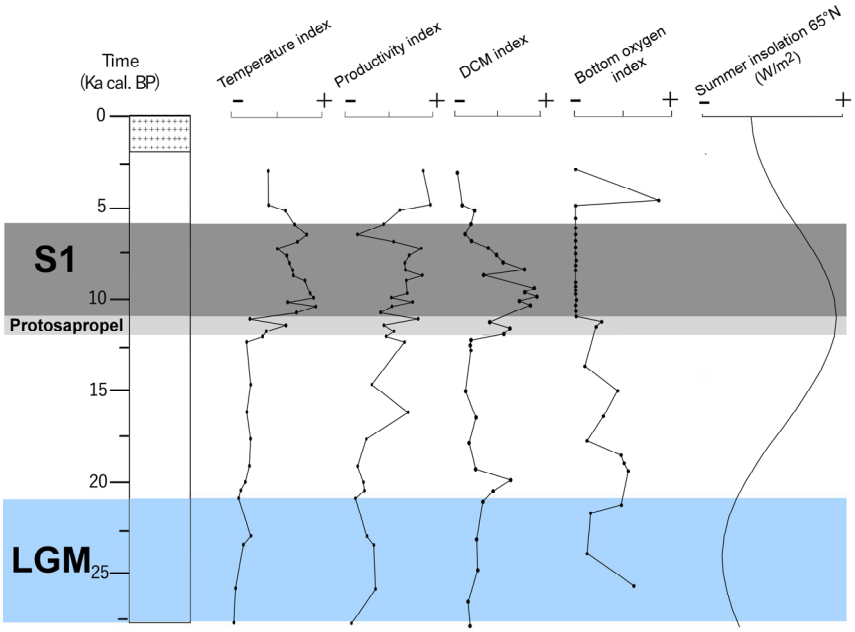

Figure 5. Micropaleontological −based and insolation indexes [58].

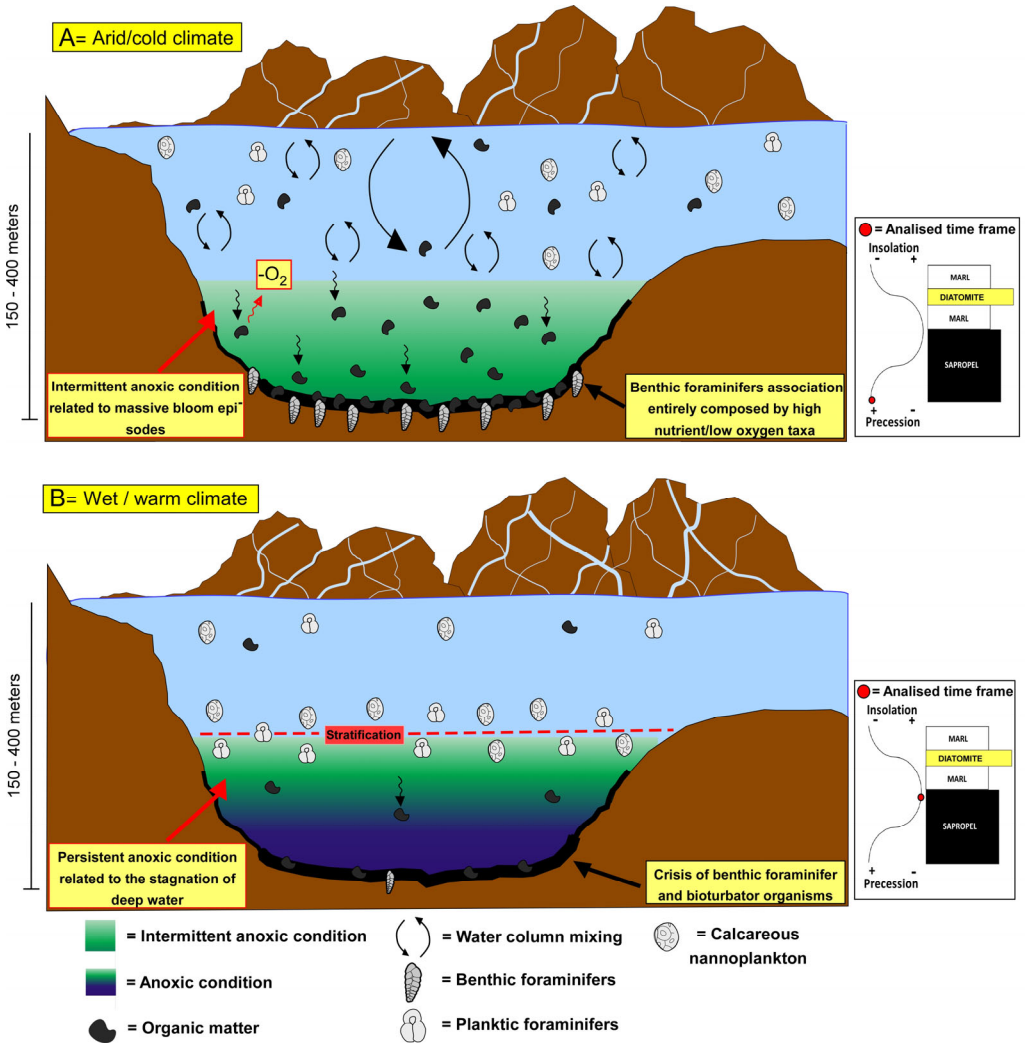

Figure 6. Sketch showing the environmental condition triggering the Messinian sapropel deposition in the Sorbas Basin based on the proxies shown in Figure 4. (**A**): During insolation minima (precession maxima), the cold temperature promoted vigorous vertical mixing and distributed the nutrient throughout the photic zone, thus stimulating primary productivity. This resulted in an increase of the organic carbon rain to the seafloor which, once re−mineralised, decreased the bottom oxygen content. (**B**): During insolation maxima (precession minima), the increase in both temperature and continental runoff favoured the stratification of the water column. Primary productivity was mostly located in the deep photic zone, where a DCM occurred. At the sea bottom, persistent anoxic conditions related to the stagnation of deep water occurred. This environmental setting led to a strong reduction or even a disappearance of benthic and bioturbator organisms.

5. Discussion

5.1. Paleoceanographic Changes of Messinian and Holocene Sapropels

Based on the data reported above, the deposition of the Messinian sapropels at Sorbas (Figure 4) started in a relatively cold context, as evidenced by the temperature indices. Cold conditions are known to promote nutrient distribution throughout the photic zone through mixing [78]. The increase of the benthic foraminiferal abundance suggests enhanced availability of organic matter on the seafloor, promoting eutrophication and the consequent oxygen consumption leading to organic matter preservation, like in the modern OMZ [79]. Thus, the Sorbas sapropels were triggered by enhanced productivity which caused oxygen deficiency at the bottom [20]. Differently, the upper portion of these sapropels is characterized by an increase in temperature and DCM indexes (Figure 4). The fine lamination characterizing the upper part of the sapropel points to an exacerbation of the oxygen starvation at the bottom, which in turn is responsible for the scarcity or absence

of benthic foraminifera (Figure 6). Indeed, benthic foraminifera are able to survive in conditions of oxygen scarcity, but if these conditions are prolonged and/or alternative electron acceptors (i.e., NO^{3-}) are scarce, their absolute abundance is negatively affected [67,80–82]. According to [49] and [20], the anoxic condition was the result of the increasing freshwater input and temperature, which promoted water column stratification (as indicated by the nannofossil-based DCM index and bottom water stagnation; Figure 4 and Figure 6). The previously applied astrochronological tuning (sapropel mid-point corresponding to insolation maxima) [36,37] was also refined based on the temperature index, placing the insolation maxima at the top of the laminated portion of the sapropel [20,60].

The deep-sea sapropel S1 of the Ionian Sea featured a different record. Literature based on detailed faunal and isotopic studies showed that deep-water stagnation progressively developed from 17 Ka cal. BP onwards and that a distinct drop in $\delta^{13}C_{benthic}$ occurred around 11 Ka cal. BP, just before the collapse of benthic ecosystems [17,83,84]. Our data showed fluctuating values and a clear absence of benthic foraminifera between 10.3 Ka cal. BP and 4.8 Ka cal. BP (Figure 5). Furthermore, the increase in temperature inferred with the paleo indices slightly below the protosapropel (Figure 5) points to a surface water warming predating the onset of the sapropel S1; this is followed by a DCM productivity increase (11.4 Ka cal. BP). creflects the water column stratification because of freshening [17,76] and references therein and warming of the surface water column that, according to our data, started well before (~1.2 Ka) than the visible S1 (10.4 Ka cal. BP). This is consistent with the freshening of the water column in the eastern Mediterranean well before the S1 onset (approximately 11.5 Ka cal BP), inferred from $\delta^{18}O$ measured on planktic foraminifera [76,85–90]. The strong time correspondence between the African Monsoon intensification, causing an increase in the fluvial discharge in the eastern Mediterranean Basin mostly through the Nile River, and the sapropel occurrence was suggested to be a pre-conditioning necessary for S1 deposition [17]. The high values of the foraminiferal productivity index that we report in the sapropel S1 (Figure 5) can be seen as consequential to increased freshwater input and nutrient delivery. In fact, according to [90], the large nutrient influx delivered by summer floods of the Nile River led to a switch from oligotrophic to meso/eutrophic state in the eastern Mediterranean, which was accompanied by enhanced primary productivity in surface waters. The transition to mesotrophic/eutrophic conditions occurred around 10 ka cal. BP [87], when precipitation and runoff in the Nile River basin peaked [91,92]. From 10 ka cal. BP onwards, a drastic increase in primary productivity has been identified in the eastern Levantine Basin [93], which suggests fertilisation of surface waters by Nile-derived nutrients [90]. These features characterising S1 are consistently recorded in other areas of the eastern Mediterranean Basin (i.e., Levantine, Aegean, and Adriatic) [17,76,88–90,94–99], and collectively suggest that the thermohaline circulation at intermediate and deep settings weakened or even stopped in response to continental runoff increase.

5.2. Sorbas Shallow-Sea vs. Holocene Deep-Sea Sapropels: What Are the Differences?

Despite a single mechanism for the sapropel formation being proposed for the Neogene and Quaternary [19], our data point to a different paleoceanographic setting characterizing sapropel in the Sorbas Basin compared with Messinian sapropels recorded elsewhere [20] and the Plio-Quaternary deep-sea sapropel record. At Sorbas, the sapropel onset shows cold eutrophic planktic foraminifera and nannofossils, and benthic foraminifera characteristic of a low-oxygen/high-nutrient environment (Figure 7) [20,49,60,61]. This microfossil association led the authors of [20] to infer that the anoxic condition was related to enhanced organic carbon export to the seafloor in response to high productivity in the water column in a relatively cold context. Basically, the Sorbas sapropel sedimentation was triggered by enhanced productivity which caused bottom anoxic condition, similarly to what is observed in a modern oxygen minimum zone, such as the coast off Perù [79] and California [100], and along the north-eastern Arabian Sea [101]. Furthermore, the Messinian sapropels in the Sorbas Basin were deposited in marginal and relatively shallow

environments, less than 300 m depth [102–107], where productivity and export pattern played a major role in controlling the oxygen bottom budget due to the proximity of the photic zone to the seafloor [20]. For instance, the last sapropel underlying the gypsum deposits (~5.99 Ma) characteristic of the Messinian Salinity Crisis event is thought to have been deposited from ~100 to 200 m of water depth [102,103,105]. Differently, most of the studied Plio-Quaternary sapropels were deposited at depth below 300 m [17 and reference therein] in response to a freshening of the surface water [17,76,86,88–90,98,99] that weakened or even stopped the oxygen delivery at intermediate and deep settings in a relatively warm/eutrophic context (Figure 7). Therefore, differently from the Sorbas sapropels, enhanced freshwater input to the basin occurred well before and preconditioned the sapropel S1 deposition through increased water stratification. Overall, the climatic and oceanographic context is completely different: at Sorbas, sapropel inception is related to high productivity in cooler condition (insolation minima) whereas the deep-sea Holocene sapropels are related to warming and freshening of the water column (insolation maxima).

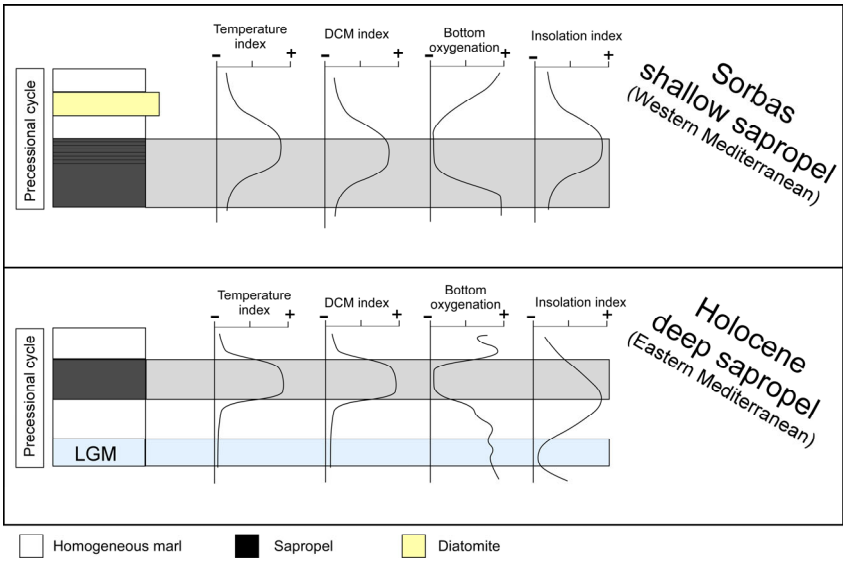

Figure 7. Comparison between the Holocene deep sapropel deposited in the eastern Mediterranean with the shallow Messinian sapropel deposited in the Sorbas Basin. The light blue rectangle at the bottom refers to the Last Glacial Maximum [LGM]. The warm/oligotrophic, cold/eutrophic, DCM, and the oxygen data are from [20, 49, 60, 61]. These indexes were based on the distribution of planktic foraminifera and nannofossils (warm/oligotrophic, cold/eutrophic and DCM index) and on benthic foraminifera (oxygen concentration) (for more detail see the Section 3.1 and Section 3.3).

5.3. A clue on Future Deoxygenation: Are Sapropels a Good Analogue?

The Mediterranean region is considered one of the most vulnerable areas impacted by climate changes, usually referred as a climate change "hot spot" [108]. Drying and warming trends have been recorded during the last decades, and they are predicted to further exacerbate in the near future [25,27,29,109–112]. As the ocean warms, a reduction of the oxygen solubility [6], a weakening of the thermohaline circulation [113,114], and an increase in the oxygen demand for microbial activity [4] occur, leading to the so-called "ocean deoxygenation" [115]. In a semi-enclosed basin such as the Mediterranean Sea, ocean deoxygenation is exacerbated by the eutrophication phenomena and the consequent instauration of hypoxic zones, which are currently expanding in the coastal areas [21,22,25]. Ocean models project for the end of this century an increase in the global mean sea surface temperature and salinity of +3.1 °C and +0.48, respectively [27], that will lead to a slowdown of the thermohaline circulation (i.e., deep-water formation) of 40% for the intermediate water, and of 80% for the deep water [27]. In the Mediterranean, the average sea surface temperature (SST) shows an increasing trend of about 0.4 °C per decade across a 30-year time interval (1986–2015) [111]. A warming trend of about 0.12 °C during the

period 1959–1988 was observed even in the deep waters of the western Mediterranean [109], increasing the deep-sea prokaryotic metabolism and thus the oxygen consumption [4]. Looking at the alkenone-based SST proxy, the temperature record of the Messinian from 6.7 to 5.9 Ma spans from 22 °C to 30 °C in the Eastern Mediterranean [116–118]. This temperature range is higher than the average SST recorded during the 1986–2015 period in the Mediterranean (14.1 °C to 24.3 °C; 111], but it fits with the temperature range predicted for the year 2100 (relative increase of 5.8° C) [111]. This match between the Messinian SST recorded in the eastern Mediterranean and the projected temperature of the near future, further supports that the Messinian paleoenvironment may represent a time window to decipher future environmental dynamics under the current climate change.

The current warming trend impacts the oceanic realm through multiple and complex dynamics; among these, the decrease in the oxygen solubility in water, the increase in stratification episodes, and the reduced thermohaline circulation ultimately resulted in the deoxygenation of Mediterranean water [2,27,114]. All these features appear to be favourable for a decrease in the oxygen content and the consequent organic carbon accumulation in the sediment (sapropel settlement). However, the current Mediterranean setting cannot be easily compared with the Mediterranean setting at the time of S1 deposition, mostly because the Nile River discharge in the Mediterranean Basin has severely decreased after the completion of the Aswan High Dam [119]. Furthermore, a regional climate model showed an increase in the freshwater deficit of +40% for the period 2070–2099 [120], mostly due to the runoff decrease of both the Po River and the outflow from the Black Sea [27]. On the other hand, a mass balance model indicates that the Eastern Mediterranean bottom water will remain fully oxygenated on time scale >100 yr, even if deep-water formation will be strongly reduced [27,28]. Furthermore, the modern insolation intensity is close to its minimum [121] and is different from the orbital configuration characterizing the onset of S1 deposition. Based on what was reported above, the bottom condition in the Mediterranean area in the near future (decadal time scale) likely will not follow the deoxygenation dynamics characteristic of the Holocene sapropel deposited in deep environments.

Nowadays, the Mediterranean is affected by eutrophication and a consequent deoxygenation pattern in several coastal and enclosed areas (Figure 1) [7,21–25]. These environments are experiencing the spreading of seasonal bottom hypoxia, in response to primary productivity peaks (generally in summer after spring bloom, when the water column stratification is strongest), sometime fuelled by riverine runoff enriched with fertilizers [7,25,122]. Algal toxic blooms and mortality of benthic organisms are often associated with eutrophication in the Mediterranean coastal area [7,22,23,25] with negative repercussions on the marine ecosystem functioning which could preclude water resource exploitation by human activities [24]. For example, in the modern north-western Adriatic coasts, the freshwater input carrying nutrients coming from the Po River causes eutrophication and bottom anoxic condition associated with huge mortality of fishes [22,123]. In this environment, eutrophic areas only occur along the coast near the river mouths and urban agglomerations [124], where fertilizers and other organic substances interact with the coastal realm. This part of the Adriatic is affected by a deterioration of the water quality: the abnormal colour of the water due to high concentration of suspended phytoplankton biomass results in poor transparency of the water combined with a smell of putrefaction [22]. In this perspective, this environment is experiencing a negative repercussion on the economy of the region (i.e., fisheries, decreasing tourism, etc.) related to oxygen deficiency.

The comparison presented In this paper evidences that although Plio-Quaternary sapropels remain an important feature to be explored to understand the interplay between high- and low-latitude climate [125], the Messinian sapropels of the Sorbas Basin, deposited on the shelf, appear to be the best analogue for the future deoxygenation scenario (i.e., end of this century) in the Mediterranean, as they record high productivity and organic carbon export to the seafloor which caused intermittent bottom oxygen deficiency (Figure

6). In this perspective, the shallow-water Sorbas sapropels represent an important source of information and can provide possible scenarios useful for the adaptation to the new incoming condition. In fact, such a mechanism potentially enhances the organic carbon burial in the bottom sediments, although the magnitude and the spatial distribution of this event varies according to the warming rate. The warming rate associated with Messinian precessional variation (from the sapropel base to the top, corresponding to insolation minima to insolation maxima; ~10 Ka) in the western Mediterranean was calculated through the Mg/Ca on planktic foraminifera and is on average ~0.001 °C year^{-1} [20]. If we compare this warming rate to the modern one, we observe that in the interval 1986–2015, an increase in the SST of about 0.04 °C year $^{-1}$ was recorded; a black box model for the interval 2071–2100 indicates a further increase in the SST of 5.8 °C compared with the period 1986–2015 (predicted warming rate of ~0.68 °C year^{-1}) [111]. Noteworthily, the calculated Messinian warming rate is two orders of magnitude lower than the warming projected by the end of this century. Although the warming rates of the natural precession-driven (extremely slow) and the anthropogenic change (extremely fast) are clearly not comparable, important information regarding the ecosystem response could be obtained and used to predict future impact scenarios. In the Sorbas Basin, during the sapropel warming phase, a decrease in the bottom oxygen led to a disappearance of bioturbator organisms (Figure 6), as reflected by the lamination of the sediment at the top of the sapropel. This because bottom oxygen deficiency also impacts the plankton and motile bioturbator communities through reduced growth and reproduction rates, reduced activity levels, increased mortality, constrained vertical migration to the oxygenated part of the water column, habitat reduction, shifts in size structure and community composition in favour of smaller individuals and egg-carrying species, and altered predator–prey dynamics, as observed in the modern setting [12,126].

Differently from the Messinian case of Sorbas, when the natural environmental change associated with deoxygenation was slow, the current environmental change rates are exceeding the adaptation potential of marine organisms to the newly established condition [14], thus increasing the magnitude of the impact. Likely, the ongoing anthropogenic climate warming and eutrophication have the potential to severely impact the benthic and sea bottom ecosystem functioning, with possible negative repercussions on the plankton community, which in turn will impact ecosystem services and marine resources, such as fisheries [122], and therefore, also human activities.

6. Conclusions

The deposition of the shallow Messinian sapropels recorded in the western Mediterranean was triggered by high primary productivity in the water column and by high organic carbon rain to the seafloor in a relatively cold context. Conversely, in the upper part of these sapropels, the condition progressively shifted to warm/humid with the instauration of vertical stratification that separated the oxygenated condition in the upper water column, and permanent anoxic condition on the seafloor. This upper portion of the sapropel is finely laminated, indicating the disappearance of bioturbator organisms. On the other hand, the Holocene sapropel was deposited as the result of a weakening/stopping of the thermohaline circulation, responsible for the deep-water renewal that provides oxygen at the sea bottom. As consistently recorded in other sites, these paleoceanographic changes were triggered by an increase in temperature and freshwater input, the latter mostly from the Nile River. Due to the modern oceanographic setting of the Mediterranean (i.e., closure of the Aswan Dam) and the predicted changes under the current climate warming (i.e., drying and warming trend), we infer that the Holocene sapropel setting is likely not comparable with near-future deoxygenation dynamics. Furthermore, oceanographic and mass balance models indicate that despite the thermohaline circulation losing its strength, the eastern Mediterranean abysses will remain well-oxygenated in the near future (end of this century). Instead, the eutrophication-driven bottom anoxic condition that characterised the onset of the sapropel deposition in the western Mediterranean

during the Messinian could be comparable to the current situation in several marginal and enclosed basins in the Mediterranean. According to the paleoceanographic change that characterises the Messinian sapropel from the base to top, corresponding to a warming phase, an exacerbation of the bottom oxygen deficiency should be expected in the future. Indeed, the Messinian case suggests that wide areas of shelf seafloors could be affected by anoxia if the warming affects eutrophicated areas. We conclude that, as climate warming will continue in the near future, an impact on the benthic and planktic communities in response to deoxygenation should be expected, as already occurred during the cyclical warming phase of the Messinian.

Supplementary Materials: The following supporting information can be downloaded at: https://www.mdpi.com/article/10.3390/jmse11030562/s1, Figure S1: Core M25/4-12; Figure S2: Calcareous nannofossils relative abundance; Figure S3: Planktic and benthic foraminifers abundance; Table S1: Radiometric age of M25/4-12.

Author Contributions: Conceptualization, A.M.M. and A.N.; methodology, A.M.M., A.N., C.M. and G.B.; validation, A.M.M., R.G., F.L., C.M. and A.N.; resources, A.M.M. and A.N., writing—original draft preparation— A.M.M.; writing—review and editing, A.M.M., R.G., F.L., C.M., G.B. and A.N.; visualization, A.M.M. All authors have read and agreed to the published version of the manuscript.

Funding: This research did not receive any specific grant from funding agencies in the public, commercial, or not-for-profit sectors.

Data Availability Statement: Data are in submission phase to PANGEA repository (temporary ticket PDI-34011.

Conflicts of Interest: The authors declare no conflict of interest.

References

1. IPCC. *Climate Change 2021: The Physical Science Basis. Contribution of Working Group I to the Sixth Assessment Report of the Intergovernmental Panel on Climate Change*; Masson-Delmotte, V., Zhai, P., Pirani, A., Connors, S.L., Péan, C., Berger, S., Caud, N., Chen, Y., Goldfarb, L., Gomis, M.I.; et al., Eds.; Cambridge University Press: Cambridge, UK; New York, NY, USA. https://doi.org/10.1017/9781009157896.
2. Limburg, K.E.; Breitburg, D.; Swaney, D.P.; Jacinto, G. Ocean deoxygenation: A primer. *One Earth* **2020**, *2*, 24–29. https://doi.org/10.1016/j.oneear.2020.01.001.
3. Mavropoulou, A.-M.; Vervatis, V.; Sofianos, S. Dissolved oxygen variability in the Mediterranean Sea. *J. Mar. Syst.* **2020**, *208*, 103348. https://doi.org/10.1016/j.jmarsys.2020.103348.
4. Danovaro, R. Climate change impacts on the biota and on vulnerable habitats of the deep Mediterranean Sea. *Rendiconti Lincei-Sci. Fis. Nat.* **2018**, *29*, 525–541. https://doi.org/10.1007/s12210-018-0725-4.
5. Robinson, C. Microbial respiration, the engine of ocean deoxygenation. *Front. Mar. Sci.* **2019**, *5*, 533. https://doi.org/10.3389/fmars.2018.00533.
6. Schmidtko, S.; Stramma, L.; Visbeck, M. Decline in global oceanic oxygen content during the past five decades. *Nature* **2017**, *542*, 335–339. https://doi.org/10.1038/nature21399.
7. Diaz, R.J.; Rosenberg, R. Spreading dead zones and consequences for marine ecosystems. *Science* **2008**, *321*, 926–929. https://doi.org/10.1126/science.1156401.
8. Stramma, L.; Schmidtko, S.; Levin, L.A.; Johnson, G.C. Ocean oxygen minima expansions and their biological impacts. *Deep Sea Res. Part I Oceanogr. Res. Pap.* **2010**, *57*, 587–595. https://doi.org/10.1016/j.dsr.2010.01.005.
9. Zhou, X.; Thomas, E.; Rickaby, R.E.M.; Winguth, A.M.E.; Lu, Z. I/Ca evidence for upper ocean deoxygenation during the PETM. *Paleoceanography* **2014**, *29*, 964–975. https://doi.org/10.1002/2014pa002702.
10. Yao, W.; Paytan, A.; Wortmann, U.G. Large-scale ocean deoxygenation during the Paleocene-Eocene Thermal Maximum. *Science* **2019**, *361*, 804–806. https://doi.org/10.1126/science.aar8658.
11. Diaz, R.J.; Rosenberg, R. Marine benthic hypoxia: A review of its ecological effects and the behavioural responses of benthic macrofauna. Oceanography and marine biology. *Annu. Rev.* **1995**, *33*, 03.
12. Roman, M.R.; Brandt, S.B.; Houde, E.D.; Pierson, J.J. Interactive effects of hypoxia and temperature on coastal pelagic zooplankton and fish. *Front. Mar. Sci.* **2019**, *6*, 139. https://doi.org/10.3389/fmars.2019.00139.
13. Pauly, D.; Dimarchopoulou, D. Introduction: Fishes in a warming and deoxygenating world. *Environ. Biol. Fishes* **2022**, *105*, 1261–1267. https://doi.org/10.1007/s10641-022-01357-y.
14. Doney, S.C.; Ruckelshaus, M.; Duffy, J.E.; Barry, J.P.; Chan, F.; English, C.A.; Galindo, H.M.; Grebmeier, J.M.; Hollowed, A.B.; Knowlton, N.; et al. Climate change impacts on marine ecosystems. *Annu. Rev. Mar. Sci.* **2012**, *4*, 11–37.

15. Kidd, R.B.; Cita, M.B.; Ryan, W.B.F. Stratigraphy of eastern Mediterranean sapropel sequences recovered during DSDP Leg 42A and their paleoenvironmental significance. *Affil. (Anal.) Lamont-Doherty Geol. Obs.* **1978**, *42*, 421.
16. Emeis, K.C.; Party, S.S. Paleoceanography and sapropel introduction. *Proc. Ocean. Drill. Program Initial. Rep.* **1996**, *160*, 21–28.
17. Rohling, E.; Marino, G.; Grant, K. Mediterranean climate and oceanography, and the periodic development of anoxic events (sapropels). *Earth-Sci. Rev.* **2015**, *143*, 62–97. https://doi.org/10.1016/j.earscirev.2015.01.008.
18. Rohling, E.J.; Hilgen, F.J. The eastern Mediterranean climate at times of sapropel formation: A review. *Neth. J. Geosci./Geol. En Mijnb.* **2007**, *70*, 253–264.
19. Schenau, S.J.; Antonarakou, A.; Hilgen, F.J.; Lourens, L.J.; Nijenhuis, I.A.; van der Weijden, C.H.; Zachariasse, W.J. Organic-rich layers in the Metochia section (Gavdos, Greece): Evidence for a single mechanism of sapropel formation during the past 10 My. *Mar. Geol.* **1999**, *153*, 117–135. https://doi.org/10.1016/s0025-3227(98)00086-3.
20. Mancini, A.M.; Gennari, R.; Ziveri, P.; Mortyn, P.G.; Stolwijk, D.J.; Lozar, F. Calcareous nannofossil and foraminiferal trace element records in the Sorbas Basin: A new piece of the Messinian Salinity Crisis onset puzzle. *Palaeogeogr. Palaeoclim. Palaeoecol.* **2020**, *554*, 109796. https://doi.org/10.1016/j.palaeo.2020.109796.
21. Justić, D.; Legović, T.; Rottini-Sandrini, L. Trends in oxygen content 1911–1984 and occurrence of benthic mortality in the northern Adriatic Sea. *Estuar. Coast. Shelf Sci.* **1987**, *25*, 435–445. https://doi.org/10.1016/0272-7714(87)90035-7.
22. UNEP-MAP. State of the Mediterranean Marine and Coastal Environment. Highlights for Policy Makers. 2012. Available online: www.unepmap.org/index.php (accessed on 02 December 2022).
23. Turley, C.M. The changing Mediterranean Sea—A sensitive ecosystem? *Prog. Oceanogr.* **1999**, *44*, 387–400. https://doi.org/10.1016/s0079-6611(99)00033-6.
24. Viaroli, P.; Nizzoli, D.; Pinardi, M.; Soana, E.; Bartoli, M. Eutrophication of the Mediterranean Sea: A watershed—Cascading aquatic filter approach. *Rend. Lince-Sci. Fis. Nat.* **2014**, *26*, 13–23. https://doi.org/10.1007/s12210-014-0364-3.
25. MedECC. *Climate and Environmental Change in the Mediterranean Basin–Current Situation and Risks for the Future*; First Mediterranean Assessment Report; Cramer, W., Guiot, J., Marini, K., Eds.; Union for the Mediterranean, Plan Bleu, UNEP/MAP: Marseille, France, 2020; 632p. https://doi.org/10.5281/zenodo.4768833.
26. Schlitzer, R. Ocean Data View, Version 4.4. 2. 2014-03-31. 2011. Available online: https://odv.awi.de (accessed on 5 October 2021).
27. Somot, S.; Sevault, F.; Déqué, M. Transient climate change scenario simulation of the Mediterranean Sea for the twenty-first century using a high-resolution ocean circulation model. *Clim. Dyn.* **2006**, *27*, 851–879. https://doi.org/10.1007/s00382-006-0167-z.
28. Powley, H.R.; Krom, M.D.; Van Cappellen, P. Circulation and oxygen cycling in the Mediterranean Sea: Sensitivity to future climate change. *J. Geophys. Res. Ocean.* **2016**, *121*, 8230–8247. https://doi.org/10.1002/2016jc012224.
29. Reale, M.; Cossarini, G.; Lazzari, P.; Lovato, T.; Bolzon, G.; Masina, S.; Solidoro, C.; Salon, S. Acidification, deoxygenation, and nutrient and biomass declines in a warming Mediterranean Sea. *Biogeosciences* **2022**, *19*, 4035–4065. https://doi.org/10.5194/bg-19-4035-2022.
30. Berger, A.L. Long-Term variations of caloric insolation resulting from the Earth's orbital elements. *Quat. Res.* **1978**, *9*, 139–167. https://doi.org/10.1016/0033-5894(78)90064-9.
31. Taylforth, J.E.; McCay, G.A.; Ellam, R.; Raffi, I.; Kroon, D.; Robertson, A.H. Middle Miocene (Langhian) sapropel formation in the easternmost Mediterranean deep-water basin: Evidence from northern Cyprus. *Mar. Pet. Geol.* **2014**, *57*, 521–536. https://doi.org/10.1016/j.marpetgeo.2014.04.015.
32. Olausson, E. Studies of deep-sea cores. *Rep. Swed. Deep Sea Exped.* **1961**, *1947–1948*, 353–391.
33. Tesi, T.; Asioli, A.; Minisini, D.; Maselli, V.; Valle, G.D.; Gamberi, F.; Langone, L.; Cattaneo, A.; Montagna, P.; Trincardi, F. Large-scale response of the Eastern Mediterranean thermohaline circulation to African monsoon intensification during sapropel S1 formation. *Quat. Sci. Rev.* **2017**, *159*, 139–154. https://doi.org/10.1016/j.quascirev.2017.01.020.
34. Pinardi, N.; Masetti, E. Variability of the large scale general circulation of the Mediterranean Sea from observations and modelling: A review. *Palaeogeogr. Palaeoclim. Palaeoecol.* **2000**, *158*, 153–173. https://doi.org/10.1016/s0031-0182(00)00048-1.
35. Krijgsman, W.; Hilgen, F.J.; Raffi, I.; Sierro, F.J.; Wilson, D.S. Chronology, causes and progression of the Messinian salinity crisis. *Nature* **1999**, *400*, 652–655. https://doi.org/10.1038/23231.
36. Hilgen, F.J.; Krijgsman, W.; Langereis, C.G.; Lourens, L.J.; Santarelli, A.; Zachariasse, W.J. Extending the astronomical (polarity) time scale into the Miocene. *Earth Planet. Sci. Lett.* **1995**, *136*, 495–510. https://doi.org/10.1016/0012-821x(95)00207-s.
37. Hilgen, F.J.; Krijgsman, W. Cyclostratigraphy and astrochronology of the Tripolo diatomite formation pre-evaporite Messinian, Sicily, Italy. *Terra Nova* **1999**, *11*, 16–22.
38. Flecker, R.; Krijgsman, W.; Capella, W.; Martíns, C.D.C.; Dmitrieva, E.; Mayser, J.P.; Marzocchi, A.; Modestou, S.; Ochoa, D.; Simon, D.; et al. Evolution of the Late Miocene Mediterranean–Atlantic gateways and their impact on regional and global environmental change. *Earth-Sci. Rev.* **2015**, *150*, 365–392. https://doi.org/10.1016/j.earscirev.2015.08.007.
39. Kouwenhoven, T.; Morigi, C.; Negri, A.; Giunta, S.; Krijgsman, W.; Rouchy, J.-M. Paleoenvironmental evolution of the eastern Mediterranean during the Messinian: Constraints from integrated microfossil data of the Pissouri Basin (Cyprus). *Mar. Micropaleontol.* **2006**, *60*, 17–44. https://doi.org/10.1016/j.marmicro.2006.02.005.
40. Corbí, H.; Soria, J.M.; Giannetti, A.; Yébenes, A. The step-by-step restriction of the Mediterranean (start, amplification, and consolidation phases) preceding the Messinian Salinity Crisis (climax phase) in the Bajo Segura basin. *Geo-Mar. Lett.* **2020**, *40*, 341–361. https://doi.org/10.1007/s00367-020-00647-7.

41. Bulian, F.; Kouwenhoven, T.J.; Jiménez-Espejo, F.J.; Krijgsman, W.; Andersen, N.; Sierro, F.J. Impact of the Mediterranean-Atlantic connectivity and the late Miocene carbon shift on deep-sea communities in the Western Alboran Basin. *Palaeogeogr. Palaeoclim. Palaeoecol.* **2022**, *589*, 110841. https://doi.org/10.1016/j.palaeo.2022.110841.
42. Hilgen, F.J.; Aziz, H.A.; Krijgsman, W.; Raffi, I.; Turco, E. Integrated stratigraphy and astronomical tuning of the Serravallian and lower Tortonian at Monte dei Corvi (Middle–Upper Miocene, northern Italy). *Palaeogeogr. Palaeoclim. Palaeoecol.* **2003**, *199*, 229–264. https://doi.org/10.1016/s0031-0182(03)00505-4.
43. Kouwenhoven, T.J.; Seidenkrantz, M.-S.; van der Zwaan, G.J. Deep-water changes: The near-synchronous disappearance of a group of benthic foraminifera from the Late Miocene Mediterranean. *Palaeogeogr. Palaeoclim. Palaeoecol.* **1999**, *152*, 259–281. https://doi.org/10.1016/s0031-0182(99)00065-6.
44. Gladstone, R.; Flecker, R.; Valdes, P.; Lunt, D.; Markwick, P. The Mediterranean hydrologic budget from a Late Miocene global climate simulation. *Palaeogeogr. Palaeoclim. Palaeoecol.* **2007**, *251*, 254–267. https://doi.org/10.1016/j.palaeo.2007.03.050.
45. Karakitsios, V.; Roveri, M.; Lugli, S.; Manzi, V.; Gennari, R.; Antonarakou, A.; Triantaphyllou, M.; Agiadi, K.; Kontakiotis, G.; Kafousia, N.; et al. A record of the Messinian salinity crisis in the eastern Ionian tectonically active domain (Greece, eastern Mediterranean). *Basin Res.* **2017**, *29*, 203–233. https://doi.org/10.1111/bre.12173.
46. Sierro, F.J.; Flores, J.A.; Zamarreño, I.; Vázquez, A.; Utrilla, R.; Francés, G.; Hilgen, F.J.; Krijgsman, W. Messinian pre-evaporite sapropels and precession-induced oscillations in western Mediterranean climate. *Mar. Geol.* **1999**, *153*, 137–146. https://doi.org/10.1016/s0025-3227(98)00085-1.
47. Iaccarino, S.M.; Bertini, A.; Di Stefano, A.; Ferraro, L.; Gennari, R.; Grossi, F.; Lirer, F.; Manzi, V.; Menichetti, E.; Lucchi, M.R.; et al. The Trave section (Monte dei Corvi, Ancona, Central Italy): An integrated paleontological study of the Messinian deposits. *Stratigraphy* **2008**, *5*, 281–306.
48. Di Stefano, A.; Verducci, M.; Lirer, F.; Ferraro, L.; Iaccarino, S.M.; Hüsing, S.K.; Hilgen, F.J. Paleoenvironmental conditions preceding the Messinian Salinity Crisis in the Central Mediterranean: Integrated data from the Upper Miocene Trave section (Italy). *Palaeogeogr. Palaeoclim. Palaeoecol.* **2010**, *297*, 37–53. https://doi.org/10.1016/j.palaeo.2010.07.012.
49. Sierro, F.J.; Flores, J.A.; Frances, G.; Vazquez, A.; Utrilla, R.; Zamarreño, I.; Erlenkeuser, H.; Barcena, M.A. Orbitally-controlled oscillations in planktic communities and cyclic changes in western Mediterranean hydrography during the Messinian. *Palaeogeogr. Palaeoclimatol. Palaeoecol.* **2003**, *190*, 289–316. https://doi.org/10.1016/s0031-0182(02)00611-9.
50. AlHammoud, B.; Meijer, P.T.; Dijkstra, H.A. Sensitivity of Mediterranean thermohaline circulation to gateway depth: A model investigation. *Paleoceanography* **2010**, *25*. https://doi.org/10.1029/2009pa001823.
51. Gennari, R.; Lozar, F.; Turco, E.; Pierre, F.D.; Lugli, S.; Manzi, V.; Natalicchio, M.; Roveri, M.; Schreiber, B.C.; Taviani, M. Integrated stratigraphy and paleoceanographic evolution of the pre-evaporitic phase of the Messinian salinity crisis in the Eastern Mediterranean as recorded in the Tokhni section (Cyprus island). *Newsl. Strat.* **2018**, *51*, 33–55. https://doi.org/10.1127/nos/2017/0350.
52. Popov, S.V.; Rogl, F.; Rozanov, A.Y.; Steininger, F.F.; Shcherba, I.G.; Kovac, M. Lithological-paleogeographic maps of paratethys. CFS Cour. *Forsch. Senckenberg* **2004**, *254*, 1–46.
53. Manzi, V.; Roveri, M.; Gennari, R.; Bertini, A.; Biffi, U.; Giunta, S.; Iaccarino, S.M.; Lanci, L.; Lugli, S.; Negri, A.; et al. The deep-water counterpart of the Messinian lower Evaporites in the Apennine foredeep: The Fanantello section (Northern Apennines, Italy). *Palaeogeogr. Palaeoclim. Palaeoecol.* **2007**, *251*, 470–499. https://doi.org/10.1016/j.palaeo.2007.04.012.
54. Lozar, F.; Violanti, D.; Pierre, F.D.; Bernardi, E.; Cavagna, S.; Clari, P.; Irace, A.; Martinetto, E.; Trenkwalder, S. Calcareous nannofossils and foraminifers herald the Messinian Salinity Crisis: The Pollenzo section (Alba, Cuneo; NW Italy). *Geobios* **2010**, *43*, 21–32. https://doi.org/10.1016/j.geobios.2009.07.002.
55. Corbí, H.; Soria, J.M.; Lancis, C.; Giannetti, A.; Tent-Manclús, J.E.; Dinarès-Turell, J. Sedimentological and paleoenvironmental scenario before, during, and after the Messinian Salinity Crisis: The San Miguel de Salinas composite section (western Mediterranean). *Mar. Geol.* **2016**, *379*, 246–266. https://doi.org/10.1016/j.margeo.2016.05.017.
56. Krijgsman, W.; Capella, W.; Simon, D.; Hilgen, F.J.; Kouwenhoven, T.J.; Meijer, P.T.; Sierro, F.J.; Tulbure, M.A.; van den Berg, B.C.; van der Schee, M.; et al. The Gibraltar Corridor: Watergate of the Messinian Salinity Crisis. *Mar. Geol.* **2018**, *403*, 238–246. https://doi.org/10.1016/j.margeo.2018.06.008.
57. Capella, W.; Flecker, R.; Hernández-Molina, F.J.; Simon, D.; Meijer, P.T.; Rogerson, M.; Sierro, F.J.; Krijgsman, W. Mediterranean isolation preconditioning the Earth System for late Miocene climate cooling. *Sci. Rep.* **2019**, *9*, 3795. https://doi.org/10.1038/s41598-019-40208-2.
58. Laskar, J.; Robutel, P.; Joutel, F.; Gastineau, M.; Correia, A.C.M.; Levrard, B. A long-term numerical solution for the insolation quantities of the Earth. *Astron. Astrophys.* **2004**, *428*, 261–285. https://doi.org/10.1051/0004-6361:20041335.
59. Sierro, F.J.; Hilgen, F.J.; Krijgsman, W.; Flores, J.A. The Abad composite (SE Spain): A Messinian reference section for the Mediterranean and the APTS. *Palaeogeogr. Palaeoclim. Palaeoecol.* **2001**, *168*, 141–169. https://doi.org/10.1016/s0031-0182(00)00253-4.
60. Pérez-Folgado, M.; Sierro, F.J.; Bárcena, M.A.; Flores, J.; Vázquez, A.; Utrilla, R.; Hilgen, F.; Krijgsman, W.; Filippelli, G. Western versus eastern Mediterranean paleoceanographic response to astronomical forcing: A high-resolution microplankton study of precession-controlled sedimentary cycles during the Messinian. *Palaeogeogr. Palaeoclim. Palaeoecol.* **2003**, *190*, 317–334. https://doi.org/10.1016/s0031-0182(02)00612-0.
61. Flores, J.-A.; Sierro, F.J.; Filippelli, G.M.; Bárcena, M..; Pérez-Folgado, M.; Vázquez, A.; Utrilla, R. Surface water dynamics and phytoplankton communities during deposition of cyclic late Messinian sapropel sequences in the western Mediterranean. *Mar. Micropaleontol.* **2005**, *56*, 50–79. https://doi.org/10.1016/j.marmicro.2005.04.002.

62. Reghizzi, M.; Gennari, R.; Douville, E.; Lugli, S.; Manzi, V.; Montagna, P.; Roveri, M.; Sierro, F.J.; Taviani, M. Isotope stratigraphy (87Sr/86Sr, δ18O, δ13C) of the Sorbas basin (Betic Cordillera, Spain): Paleoceanographic evolution across the onset of the Messinian salinity crisis. *Palaeogeogr. Palaeoclim. Palaeoecol.* **2017**, *469*, 60–73. https://doi.org/10.1016/j.palaeo.2016.12.039.
63. Hemleben, C.; Spindler, M.; Anderson, O.R. *Modern Planktonic Foraminifera*; Springer: New York, NY, USA, 1989; pp. 1–363. https://doi.org/10.1007/978-1-4612-3544-6.
64. Pujol, C.; Grazzini, C.V. Distribution patterns of live planktic foraminifers as related to regional hydrography and productive systems of the Mediterranean Sea. *Mar. Micropaleontol.* **1995**, *25*, 187–217. https://doi.org/10.1016/0377-8398(95)00002-i.
65. Jannink, N.T.; Zachariasse, W.J.; Van Der Zwaan, G.J. Living (Rose Bengal stained) benthic foraminifera from the Pakistan continental margin (northern Arabian Sea). *Deep Sea Res. Part I Oceanogr. Res. Pap.* **1998**, *45*, 1483–1513. https://doi.org/10.1016/s0967-0637(98)00027-2.
66. Jorissen, F.J. Benthic foraminiferal microhabitats below the sediment-water interface. In *Modern Foraminifera*; Springer: Dordrecht, The Netherlands, 1999; pp. 161–179. https://doi.org/10.1007/0-306-48104-9_10.
67. Murray, J.W. *Ecology and Applications of Benthic Foraminifera*; Cambridge University Press: Cambridge, UK, 2006; pp. 1–426.
68. Morigi, C.; Jorissen, F.J.; Gervais, A.; Guichard, S.; Borsetti, A.M. Benthic foraminiferal faunas in surface sediments off NW Africa: Relationship with organic flux to the ocean floor. *J. Foraminifer. Res.* **2001**, *31*, 350–368. https://doi.org/10.2113/0310350.
69. Morigi, C. Benthic environmental changes in the Eastern Mediterranean Sea during sapropel S5 deposition. *Palaeogeogr. Palaeoclim. Palaeoecol.* **2009**, *273*, 258–271. https://doi.org/10.1016/j.palaeo.2008.10.010.
70. Gibbs, S.; Shackleton, N.; Young, J. Orbitally forced climate signals in mid-Pliocene nannofossil assemblages. *Mar. Micropaleontol.* **2004**, *51*, 39–56. https://doi.org/10.1016/j.marmicro.2003.09.002.
71. Negri, A.; Capotondi, L.; Keller, J. Calcareous nannofossils, planktonic foraminifera and oxygen isotopes in the late Quaternary sapropels of the Ionian Sea. *Mar. Geol.* **1999**, *157*, 89–103. https://doi.org/10.1016/s0025-3227(98)00135-2.
72. Fallon, M.F.; Papadopoulos, G.; Leonard, J.J.; Patrikalakis, N.M. Cooperative AUV navigation using a single maneuvering surface craft. *Int. J. Robot. Res.* **2010**, *29*, 1461–1474. https://doi.org/10.1177/0278364910380760.
73. De Lange, G.J.; Thomson, J.; Reitz, A.; Slomp, C.P.; Principato, M.S.; Erba, E.; Corselli, C. Synchronous basin-wide formation and redox-controlled preservation of a Mediterranean sapropel. *Nat. Geosci.* **2008**, *1*, 606–610. https://doi.org/10.1038/ngeo283.
74. Keller, J.; Ryan, W.B.F.; Ninkovich, D.; Altherr, R. Explosive volcanic activity in the Mediterranean over the past 200,000 yr as recorded in deep-sea sediments. *GSA Bull.* **1978**, *89*, 591–604. https://doi.org/10.1130/0016-7606(1978)89<591:evaitm>2.0.co;2.
75. Rohling, E.J.; Sprovieri, M.; Cane, T.R.; Casford, J.S.L.; Cooke, S.; Bouloubassi, I.; Emeis, K.C.; Schiebel, R.; Rogerson, M.; Hayes, A.; et al. Reconstructing past planktic foraminiferal habitats using stable isotope data: A case history for Mediterranean sapropel S5. *Mar. Micropaleontol.* **2004**, *50*, 89–123. https://doi.org/10.1016/s0377-8398(03)00068-9.
76. Castradori, D. Calcareous nannofossils and the origin of eastern Mediterranean sapropels. *Paleoceanography* **1993**, *8*, 459–471. https://doi.org/10.1029/93pa00756.
77. Triantaphyllou, M.; Ziveri, P.; Gogou, A.; Marino, G.; Lykousis, V.; Bouloubassi, I.; Emeis, K.-C.; Kouli, K.; Dimiza, M.; Rosell-Melé, A.; et al. Late Glacial–Holocene climate variability at the south-eastern margin of the Aegean Sea. *Mar. Geol.* **2009**, *266*, 182–197. https://doi.org/10.1016/j.margeo.2009.08.005.
78. Kemp, A.E.; Pike, J.; Pearce, R.B.; Lange, C.B. The "Fall dump"—A new perspective on the role of a "shade flora" in the annual cycle of diatom production and export flux. *Deep Sea Res. Part II Top. Stud. Oceanogr.* **2000**, *47*, 2129–2154.
79. Brodie, I.; Kemp, A.E.S. Variation in biogenic and detrital fluxes and formation of laminae in late Quaternary sediments from the Peruvian coastal upwelling zone. *Mar. Geol.* **1994**, *116*, 385–398. https://doi.org/10.1016/0025-3227(94)90053-1.
80. Gooday, A.J. Benthic foraminifera (*Protista*) as tools in deep-water palaeoceanography: Environmental influences on faunal characteristics. *Adv. Mar. Biol.* **2003**, *46*, 1–90. https://doi.org/10.1016/s0065-2881(03)46002-1.
81. Bernhard, J.M.; Sen Gupta, B.K. Foraminifera of oxygen-depleted environments. In *Modern Foraminifera*; Springer: Dordrecht, The Netherlands, 2003; pp. 201–216.
82. Glock, N.; Roy, A.-S.; Romero, D.; Wein, T.; Weissenbach, J.; Revsbech, N.P.; Høgslund, S.; Clemens, D.; Sommer, S.; Dagan, T. Metabolic preference of nitrate over oxygen as an electron acceptor in foraminifera from the Peruvian oxygen minimum zone. *Proc. Natl. Acad. Sci. USA* **2019**, *116*, 2860–2865. https://doi.org/10.1073/pnas.1813887116.
83. Cornuault, M.; Tachikawa, K.; Vidal, L.; Guihou, A.; Siani, G.; Deschamps, P.; Bassinot, F.; Revel, M. Circulation Changes in the Eastern Mediterranean Sea Over the Past 23,000 Years Inferred From Authigenic Nd Isotopic Ratios. *Paleoceanography* **2018**, *33*, 264–280. https://doi.org/10.1002/2017pa003227.
84. Schmiedl, G.; Kuhnt, T.; Ehrmann, W.; Emeis, K.-C.; Hamann, Y.; Kotthoff, U.; Dulski, P.; Pross, J. Climatic forcing of eastern Mediterranean deep-water formation and benthic ecosystems during the past 22 000 years. *Quat. Sci. Rev.* **2010**, *29*, 3006–3020. https://doi.org/10.1016/j.quascirev.2010.07.002.
85. Rossignol-Strick, M. African monsoons, an immediate climate response to orbital insolation. *Nature* **1983**, *304*, 46–49. https://doi.org/10.1038/304046a0.
86. Casford, J.S.L.; Rohling, E.J.; Abu-Zied, R.; Cooke, S.; Fontanier, C.; Leng, M.; Lykousis, V. Circulation changes and nutrient concentrations in the late Quaternary Aegean Sea: A nonsteady state concept for sapropel formation. *Paleoceanography* **2002**, *17*, 14–1–14-11. https://doi.org/10.1029/2000pa000601.
87. Abu-Zied, R.H.; Rohling, E.J.; Jorissen, F.J.; Fontanier, C.; Casford, J.S.L.; Cooke, S. Benthic foraminiferal response to changes in bottom-water oxygenation and organic carbon flux in the eastern Mediterranean during LGM to Recent times. *Mar. Micropaleontol.* **2008**, *67*, 46–68. https://doi.org/10.1016/j.marmicro.2007.08.006.

88. Marino, G.; Rohling, E.J.; Sangiorgi, F.; Hayes, A.; Casford, J.S.L.; Lotter, A.F.; Kucera, M.; Brinkhuis, H. Early and middle Holocene in the Aegean Sea: Interplay between high and low latitude climate variability. *Quat. Sci. Rev.* **2009**, *28*, 3246–3262. https://doi.org/10.1016/j.quascirev.2009.08.011.
89. Hennekam, R.; Jilbert, T.; Schnetger, B.; de Lange, G.J. Solar forcing of Nile discharge and sapropel S1 formation in the early to middle Holocene eastern Mediterranean. *Paleoceanography* **2014**, *29*, 343–356. https://doi.org/10.1002/2013pa002553.
90. Blanchet, C.L.; Tjallingii, R.; Schleicher, A.M.; Schouten, S.; Frank, M.; Brauer, A. Deoxygenation dynamics on the western Nile deep-sea fan during sapropel S1 from seasonal to millennial timescales. *Clim. Past* **2021**, *17*, 1025–1050. https://doi.org/10.5194/cp-17-1025-2021.
91. Castañeda, I.S.; Schouten, S.; Pätzold, J.; Lucassen, F.; Kasemann, S.; Kuhlmann, H.; Schefuß, E. Hydroclimate variability in the Nile River Basin during the past 28,000 years. *Earth Planet. Sci. Lett.* **2016**, *438*, 47–56. https://doi.org/10.1016/j.epsl.2015.12.014.
92. Weldeab, S.; Menke, V.; Schmiedl, G. The pace of East African monsoon evolution during the Holocene. *Geophys. Res. Lett.* **2014**, *41*, 1724–1732. https://doi.org/10.1002/2014gl059361.
93. Mojtahid, M.; Manceau, R.; Schiebel, R.; Hennekam, R.; de Lange, G.J. Thirteen thousand years of southeastern Mediterranean climate variability inferred from an integrative planktic foraminiferal-based approach. *Paleoceanography* **2015**, *30*, 402–422. https://doi.org/10.1002/2014pa002705.
94. Mercone, D.; Thomson, J.; Croudace, I.W.; Siani, G.; Paterne, M.; Troelstra, S. Duration of S1, the most recent sapropel in the eastern Mediterranean Sea, as indicated by accelerator mass spectrometry radiocarbon and geochemical evidence. *Paleoceanography* **2000**, *15*, 336–347. https://doi.org/10.1029/1999pa000397.
95. Rohling, E.J.; Cane, T.R.; Cooke, S.; Sprovieri, M.; Bouloubassi, I.; Emeis, K.C.; Schiebel, R.; Kroon, D.; Jorissen, F.J.; Lorre, A.; et al. African monsoon variability during the previous interglacial maximum. *Earth Planet. Sci. Lett.* **2002**, *202*, 61–75. https://doi.org/10.1016/s0012-821x(02)00775-6.
96. Giunta, S.; Negri, A.; Morigi, C.; Capotondi, L.; Combourieu-Nebout, N.; Emeis, K.C.; Sangiorgi, F.; Vigliotti, L. Coccolithophorid ecostratigraphy and multi-proxy paleoceanographic reconstruction in the Southern Adriatic Sea during the last deglacial time (Core AD91-17). *Palaeogeogr. Palaeoclimatol. Palaeoecol.* **2003**, *190*, 39–59. http://doi.org/10.1029/2006GL025734.
97. Casford, J.S.L.; Abu-Zied, R.; Rohling, E.J.; Cooke, S.; Fontanier, C.; Leng, M.; Millard, A.; Thomson, J. A strat-igraphically controlled multi-proxy chronostratigraphy for the eastern Mediterranean. *Paleoceanography* **2007**, *22*, PA4215. http://doi.org/10.1029/2007PA001422.
98. Mojtahid, M.; Hennekam, R.; De Nooijer, L.; Reichart, G.-J.; Jorissen, F.; Boer, W.; Le Houedec, S.; De Lange, G. Evaluation and application of foraminiferal element/calcium ratios: Assessing riverine fluxes and environmental conditions during sapropel S1 in the southeastern Mediterranean. *Mar. Micropaleontol.* **2019**, *153*, 101783. https://doi.org/10.1016/j.marmicro.2019.101783.
99. Cascella, A.; Bonomo, S.; Lirer, F.; Margaritelli, G.; Checa, H.; Cacho, I.; Pena, L.D.; Frigola, J. The response of calcareous plankton to the Sapropel S1 interval in North Ionian Sea. *Glob. Planet. Chang.* **2021**, *205*, 103599. https://doi.org/10.1016/j.gloplacha.2021.103599.
100. Schimmelmann, A.; Lange, C.B. Tales of 1001 varves: A review of Santa Barbara Basin sediment studies. In *Palaeoclimatology and Palaeoceanography from Laminated Sediments*; Kemp, A.E.S., Ed.; Geological Society of London Special Publication: London, UK, 1996; Volume 116, pp. 121–141. https://doi.org/10.1144/gsl.sp.1996.116.01.12.
101. Lückge, A.; Horsfield, B.; Littke, R.; Scheeder, G. Organic matter preservation and sulfur uptake in sediments from the continental margin off Pakistan. *Org. Geochem.* **2002**, *33*, 477–488. https://doi.org/10.1016/s0146-6380(01)00171-1.
102. Dronkert, H. Late Miocene evaporites in the Sorbas Basin and adjoining areas. *Mem. Soc. Geol. Ital.* **1976**, *16*, 341–361.
103. Troelstra, S.R.; Van Der Poel, H.M.; Huisman, C.H.A.; Geerlings, L.P.; Dronkert, H. Paleoecological changes in the latest Miocene of Sorbas basin, S.E. Spain. *Géologie Méditerranéenne* **1980**, *7*, 115–125. https://doi.org/10.3406/geolm.1980.1132.
104. van de Poel, H.M. Foraminiferal biostratigraphy and palaeoenvironments of the Miocene-Pliocene Carboneras-Nijar basin (SE Spain). *Scr. Geol.* **1992**, *102*, 1–32.
105. Baggley, K.A. The late tortonian-early messinian foraminiferal record of the Abad Member (Turre formation), Sorbas Basin, Almeria, south-east Spain. *Palaeontology* **2000**, *43*, 1069–1112. https://doi.org/10.1111/1475-4983.00162.
106. Clauzon, G.; Suc, J.-P.; Couto, D.D.; Jouannic, G.; Melinte-Dobrinescu, M.C.; Jolivet, L.; Quillévéré, F.; Lebret, N.; Mocochain, L.; Popescu, S.-M.; et al. New insights on the Sorbas Basin (SE Spain): The onshore reference of the Messinian salinity crisis. *Mar. Pet. Geol.* **2015**, *66*, 71–100. https://doi.org/10.1016/j.marpetgeo.2015.02.016.
107. Modestou, S.; Simon, D.; Gutjahr, M.; Marzocchi, A.; Kouwenhoven, T.J.; Ellam, R.M.; Flecker, R. Precessional variability of $^{87}Sr/^{86}Sr$ in the late Miocene Sorbas Basin: An interdisciplinary study of drivers of interbasin exchange. *Paleoceanography* **2017**, *32*, 531–552. https://doi.org/10.1002/2016pa003061.
108. Giorgi, F. Climate change hot-spots. *Geophys. Res. Lett.* **2006**, *33*, L08707. https://doi.org/10.1029/2006GL025734
109. Bethoux, J.P.; Gentili, B.; Raunet, J.; Tailliez, D. Warming trend in the western Mediterranean deep water. *Nature* **1990**, *347*, 660–662. https://doi.org/10.1038/347660a0.
110. Nykjaer, L. Mediterranean Sea surface warming 1985–2006. *Clim. Res.* **2009**, *39*, 11–17. https://doi.org/10.3354/cr00794.
111. Sakalli, A. Sea surface temperature change in the Mediterranean Sea under climate change: A linear model for simulation of the sea surface temperature up to 2100. *Appl. Ecol. Environ. Res.* **2017**, *15*, 707–716. https://doi.org/10.15666/aeer/1501_707716.
112. Lionello, P.; Scarascia, L. The relation between climate change in the Mediterranean region and global warming. *Reg. Environ. Chang.* **2018**, *18*, 1481–1493. https://doi.org/10.1007/s10113-018-1290-1.

113. Skliris, N. Past, Present and future patterns of the thermohaline circulation and characteristic water masses of the Mediterranean Sea. In *The Mediterranean Sea*; Springer: Dordrecht, The Netherlands, 2014; pp. 29–48. https://doi.org/10.1007/978-94-007-6704-1_3.
114. Coppola, L.; Legendre, L.; Lefevre, D.; Prieur, L.; Taillandier, V.; Riquier, E.D. Seasonal and inter-annual variations of dissolved oxygen in the northwestern Mediterranean Sea (DYFAMED site). *Prog. Oceanogr.* **2018**, *162*, 187–201. https://doi.org/10.1016/j.pocean.2018.03.001.
115. Keeling, R.F.; Körtzinger, A.; Gruber, N. Ocean deoxygenation in a warming world. *Annu. Rev. Mar. Sci.* **2010**, *2*, 199–229. https://doi.org/10.1146/annurev.marine.010908.163855.
116. Tzanova, A.; Herbert, T.D.; Peterson, L. Cooling Mediterranean Sea surface temperatures during the Late Miocene provide a climate context for evolutionary transitions in Africa and Eurasia. *Earth Planet. Sci. Lett.* **2015**, *419*, 71–80. https://doi.org/10.1016/j.epsl.2015.03.016.
117. Vasiliev, I.; Karakitsios, V.; Bouloubassi, I.; Agiadi, K.; Kontakiotis, G.; Antonarakou, A.; Triantaphyllou, M.; Gogou, A.; Kafousia, N.; De Rafélis, M.; et al. Large Sea Surface Temperature, Salinity, and Productivity-Preservation Changes Preceding the Onset of the Messinian Salinity Crisis in the Eastern Mediterranean Sea. *Paleoceanogr. Paleoclimatol.* **2019**, *34*, 182–202. https://doi.org/10.1029/2018pa003438.
118. Kontakiotis, G.; Butiseacă, G.A.; Antonarakou, A.; Agiadi, K.; Zarkogiannis, S.D.; Krsnik, E.; Besiou, E.; Zachariasse, W.J.; Lourens, L.; Thivaiou, D.; et al. Hypersalinity accompanies tectonic restriction in the eastern Mediterranean prior to the Messinian Salinity Crisis. *Palaeogeogr. Palaeoclim. Palaeoecol.* **2022**, *592*, 110903. https://doi.org/10.1016/j.palaeo.2022.110903.
119. Rohling, E.J.; Bryden, H.L. Man-induced salinity and temperature increases in Western Mediterranean Deep Water. *J. Geophys. Res. Atmos.* **1992**, *97*, 11191–11198. https://doi.org/10.1029/92jc00767.
120. Sanchez-Gomez, E.; Somot, S.; Mariotti, A. Future changes in the Mediterranean water budget projected by an ensemble of regional climate models. *Geophys. Res. Lett.* **2009**, *36*. https://doi.org/10.1029/2009gl040120.
121. Wu, C.-H.; Lee, S.-Y.; Tsai, P.-C. Role of eccentricity in early Holocene African and Asian summer monsoons. *Sci. Rep.* **2021**, *11*, 24089. https://doi.org/10.1038/s41598-021-03525-z.
122. Breitburg, D.; Levin, L.A.; Oschlies, A.; Grégoire, M.; Chavez, F.P.; Conley, D.J.; Garçon, V.; Gilbert, D.; Gutiérrez, D.; Isensee, K.; et al. Declining oxygen in the global ocean and coastal waters. *Science* **2018**, *359*, eaam7240. https://doi.org/10.1126/science.aam7240.
123. Mancini, L.; Milandri, A.; Nizzoli, C.; Pirini, M.; Poletti, R.; Pompei, M.; Viviani, R. L'eutrofizzazione in rapporto ad alcuni aspetti igienico-sanitari delle acque costiere e dei prodotti della pesca. *Nova Thalass.* **1986**, *8*, 325–330.
124. Artegiani, A.; Solazzi, A.; Tolomio, C.; Marzocchi, M.; Favero, P.; Cavolo, F. Parametri fisico-chimici e fitoplancton in una stazione a Sud del Conero (Zona di ripopolamento). *Convegno Sci. Naz. PF Oceanogr. CNR* **1979**, *5*, 1979.
125. Colleoni, F.; Masina, S.; Negri, A.; Marzocchi, A. Plio–Pleistocene high–low latitude climate interplay: A Mediterranean point of view. *Earth Planet. Sci. Lett.* **2012**, *319–320*, 35–44. https://doi.org/10.1016/j.epsl.2011.12.020.
126. Batziakas, S.; Frangoulis, C.; Tsiola, A.; Nikolioudakis, N.; Tsagaraki, T.M.; Somarakis, S. Hypoxia changes the shape of the biomass size spectrum of planktonic communities: A case study in the eastern Mediterranean (Elefsina Bay). *J. Plankton Res.* **2020**, *42*, 752–766. https://doi.org/10.1093/plankt/fbaa055.